

# **Perturbation efficiency resolves target-count bias in network proximity metrics: A controlled audit**

Antony Bevan<sup>1,\*</sup>

<sup>1</sup>Department of Pharmacognosy, Madurai Medical College, Madurai, India

\*Corresponding author: antonybevan04@gmail.com

## 4 Abstract

5 Network-based metrics are essential for identifying drug–disease associations, assuming that proximity  
6 within protein–protein interaction networks reflects functional relevance. However, proximity Z-scores  
7 are fundamentally sensitive to target set size. This introduces a systematic bias where compounds with  
8 broad polypharmacology appear statistically significant due to null distribution tightening (the Law of  
9 Large Numbers) rather than physical reachability. We systematically audit this bias using the human liver  
10 interactome and constituents from *Hypericum perforatum*. We demonstrate that proximity Z-scores yield  
11 unstable rankings that reverse across network construction parameters. While compounds with many tar-  
12 gets may achieve higher significance, they can remain physically more distant from disease modules than  
13 high-leverage modulators. We resolve this by utilizing random walk–based influence propagation and in-  
14 troducing *perturbation efficiency* to ensure unbiased comparisons. Our results show that influence-based  
15 rankings are stable and correctly identify high-leverage modulators that proximity metrics miss. This  
16 study provides a methodological template for identifying and correcting statistical artifacts in network  
17 medicine, enabling reliable assessments in complex biological systems.

**Keywords:** network medicine, proximity metrics, metric robustness, drug-induced liver injury, Z-score bias, perturbation efficiency.

20 1 Introduction

<sup>21</sup> Network-based prioritization is a cornerstone of modern systems biology and drug discovery, assuming  
<sup>22</sup> that the topological proximity between compound targets and disease genes within a protein–protein in-

teraction (PPI) network reflects functional relevance [1–4]. Because raw network distances are sensitive to local topology and degree distribution, they are typically reported as Z-scores relative to degree-matched null models. While these Z-scores successfully quantify statistical significance in most applications [3], we demonstrate they can be confounded by large asymmetries in target set size. As the number of seed nodes increases, the variance of the null distribution decreases (the Law of Large Numbers), leading to deterministic significance inflation for compounds with broad polypharmacology. Identifying whether such results reflect true biological influence, or whether they represent systematic artifacts of distance-based inference, is essential for the reliability of network medicine.

Using the human liver interactome as a model system, we investigate this confounding effect through a controlled comparison of two constituents from *Hypericum perforatum* (St. John’s Wort). These constituents—Hyperforin and Quercetin—exhibit highly asymmetric target set sizes: Hyperforin possesses 10 validated targets, while Quercetin has over 60 [5–7]. This system serves as a controlled model because it pairs a known biological ground truth (Hyperforin-mediated PXR activation) with extreme topological asymmetry, providing a sharp stress test for network metrics. Conventional proximity Z-scores predict greater disease-associated significance for the broad-spectrum modulator, even when it is physically more distant from the disease module than the high-leverage modulator. This reversal indicates that proximity-based prioritization is unstable across network construction parameters and susceptible to sample-size artifacts.

Here, we evaluate the robustness of proximity-based and influence-based metrics for comparative prioritization. We demonstrate that proximity Z-scores yield unstable, threshold-dependent rankings driven by null-distribution tightening rather than physical reachability. To resolve this instability, we utilize random walk-based influence propagation, which integrates over the entire network topology and captures signal amplification through regulatory hubs [8]. We apply a normalized metric, perturbation efficiency, to account for target set size and ensure unbiased comparisons. Our results show that influence-based propagation provides a stable, theoretically consistent framework for network pharmacology that correctly identifies high-leverage perturbations where traditional proximity metrics fail.

## 2 Results

### 2.1 Proximity Z-scores are confounded by target set size

We first established network context by quantifying target count and shortest-path proximity to 82 DILI-associated genes (Figure 1). Quercetin engages 62 targets in the liver-expressed largest connected

53 component; Hyperforin engages 10. At STRING confidence  $\geq 900$ , Hyperforin targets are physically  
54 closer to DILI genes ( $d_c = 1.30$ ) than Quercetin targets ( $d_c = 1.68$ ; Table 1). However, the proxim-  
55 ity Z-scores yield the opposite ranking: Quercetin achieves  $Z = -5.44$  ( $p < 0.001$ ), while Hyperforin  
56 achieves  $Z = -3.86$  ( $p < 0.001$ ). All reported associations survived Benjamini–Hochberg FDR correc-  
57 tion ( $q < 0.05$ ).

58 This statistical artifact suggests that Quercetin poses greater risk, whereas the physical topology fa-  
59 vors Hyperforin. This effect occurs independently of network construction parameters and represents a  
60 fundamental statistical property of averaged distributions: larger samples inherently produce more pre-  
61 cise (narrower) null distributions, artificially inflating Z-score magnitude regardless of actual topological  
62 proximity. This is a manifestation of the Law of Large Numbers (LLN).

## 63 **2.2 Influence-based rankings are stable and resolve the confound**

64 Random walk with restart (RWR) stabilizes this ranking by integrating over all paths (Figure 2). Hyper-  
65 forin achieves influence  $Z = +10.12$  ( $p < 0.001$ ); Quercetin achieves  $Z = +4.55$  ( $p < 0.001$ ; Table 1).  
66 Unlike proximity, influence Z-scores correctly reflect the topological advantage of Hyperforin’s regu-  
67 latory hub occupancy. This ranking aligns with the known biological ground truth: Hyperforin is the  
68 hepatotoxic constituent responsible for drug-drug interactions via PXR activation, while Quercetin has  
69 no documented hepatotoxicity and may be hepatoprotective. The ranking remains consistent across  
70 topology-only and expression-weighted analyses, demonstrating that influence propagation is less sus-  
71 ceptible to sample-size artifacts than shortest-path distance.

## 72 **2.3 Expression weighting refines the signal**

73 To assess whether the RWR signal persists under tissue-specific constraint, we applied expression-  
74 weighted influence propagation (EWI), weighting transitions by destination-node liver expression (Fig-  
75 ure 3).

76 The Z-score differential narrows but remains substantial under expression weighting: Hyperforin  
77  $Z = +8.98$  ( $p < 0.001$ ); Quercetin  $Z = +5.79$  ( $p < 0.001$ ). Hyperforin’s advantage is driven primarily  
78 by the PXR–CYP master regulatory axis, which remains highly active in liver tissue (e.g., CYP3A4 at  
79 335 TPM). Quercetin’s influence is moderated by its broad, diffuse target profile, which includes several  
80 high-expression nodes (e.g., CFB at 1,115 TPM) that do not converge on a DILI effector hub.

81 **2.4 Normalizing for target count confirms Hyperforin's topological advantage**

82 To resolve the target-count paradox, we compared the average network influence of each individual  
83 target, reframing polypharmacology as an efficiency problem rather than a coverage problem (Figure 4;  
84 Table 2).

Compound	Targets	Eff. (RWR)	Eff. (EWI)	RWR Ratio*	EWI Ratio†
Hyperforin	10	0.1138	0.1330	—	—
Quercetin	62	0.0322	0.0493	—	—
<b>Fold difference</b>	—	—	—	<b>3.5× (3.7×)</b>	<b>2.7× (2.8×)</b>

85 \*RWR Ratio: observed ratio (robust ratio in parentheses). †EWI Ratio: observed ratio (robust ratio in paren-  
86 theses).

87 Each Hyperforin target contributes 3.7× more DILI-directed influence than each Quercetin target (robust ra-  
88 tio). This disparity indicates that Hyperforin's target positions are substantially higher leverage than those of  
89 Quercetin, achieving greater perturbation efficiency despite a 6-fold smaller target set. The efficiency ratio re-  
90 mains stable within a narrow range: 3.7× at STRING  $\geq 700$ , 3.5× at  $\geq 900$  (a 5% variation despite 33% reduction  
91 in network density). In contrast, proximity Z-score rankings undergo complete reversal between these thresholds.  
92 This demonstrates that perturbation efficiency is a parameter-invariant comparative metric where distance-based  
93 Z-scores are not.

94 **2.5 Bootstrap resampling excludes target-selection bias**

95 To rule out the possibility that Hyperforin's advantage arises from favorable target selection rather than strategic  
96 network positioning, we performed bootstrap sensitivity analysis (Figure 5). 100 random 10-target subsets were  
97 sampled without replacement from Quercetin's 62-target pool and scored by RWR.

98 Hyperforin's observed influence (0.1138) exceeds the entire bootstrap distribution from Quercetin (mean =  
99 0.0308, 95% CI = [0.0160, 0.0542]; Supplementary Table S10). The fold difference between Hyperforin and the  
100 bootstrap mean is 3.7×. This confirms that Hyperforin's advantage is not an artifact of target count; even when  
101 sampling equalized subsets from Quercetin's pool, no configuration matches Hyperforin's influence.

102 **2.6 Ranking stability across network thresholds**

103 The influence ranking is stable across network confidence thresholds (Supplementary Table S13). Hyperforin  
104 ranks first in all RWR and EWI configurations at both  $\geq 700$  and  $\geq 900$  thresholds. Notably, the proximity ranking  
105 reverses between thresholds: at  $\geq 700$ , Hyperforin is physically closer ( $d_c = 0.60$  vs 1.34) and more "significant"  
106 ( $Z = -6.04$  vs  $-5.46$ ). At  $\geq 900$ , Quercetin appears more "significant" ( $Z = -5.44$  vs  $-3.86$ ) despite being

<sup>108</sup> physically more distant (1.68 vs 1.30). This instability in proximity Z-scores—while influence rankings remain  
<sup>109</sup> stable—demonstrates that influence-based metrics are more robust to network construction parameters.

## <sup>110</sup> **2.7 Chemical similarity excludes structural confounding**

<sup>111</sup> To exclude the possibility that Hyperforin’s network signal reflects structural similarity to known hepatotoxins,  
<sup>112</sup> we performed chemical similarity analysis against the DILIrank reference set (Figure 6). Morgan fingerprints  
<sup>113</sup> (ECFP4) revealed that neither compound exceeds the 0.4 Tanimoto threshold for structural analog detection. No-  
<sup>114</sup> tably, Quercetin exhibits higher structural similarity to DILI reference drugs yet lower network influence, reinforc-  
<sup>115</sup> ing that the observed asymmetry is driven by network topology rather than chemical features.

## <sup>116</sup> **3 Discussion**

### <sup>117</sup> **3.1 Ranking stability and the Z-score confound**

<sup>118</sup> The results of this study highlight a potential limitation in the use of network proximity Z-scores when comparing  
<sup>119</sup> compounds with asymmetric target set sizes. While proximity is a standard prioritization criterion, our analysis  
<sup>120</sup> demonstrates that its significance rankings can be influenced by the target count rather than topological distance  
<sup>121</sup> alone. As the number of targets increases, the variance of the null distribution decreases (a manifestation of the Law  
<sup>122</sup> of Large Numbers), which can lead to inflated significance levels for compounds with broad polypharmacology. In  
<sup>123</sup> our controlled comparison, this effect causes a reversal of proximity-based rankings between network thresholds,  
<sup>124</sup> failing to accurately reflect the physical distance advantage of a high-leverage modulator.

<sup>125</sup> Influence-based metrics (RWR and EWI) appear less sensitive to this particular artifact. By integrating over the  
<sup>126</sup> entire network topology, these methods capture signal propagation through regulatory hubs, providing rankings that  
<sup>127</sup> remain stable across different network construction parameters. This relative stability suggests that influence-based  
<sup>128</sup> propagation may offer a more robust framework for comparative network medicine, particularly in the presence of  
<sup>129</sup> incomplete or asymmetric pharmacological data.

<sup>130</sup> The mechanistic explanation for this robustness is that RWR integrates over *all* paths, capturing how signals  
<sup>131</sup> amplify through hubs like PXR and AKT1. Shortest-path proximity, by contrast, is a descriptive metric for min-  
<sup>132</sup> imum reachability; treating it as an inferential surrogate for functional impact conflates topological context with  
<sup>133</sup> biological consequence.

### <sup>134</sup> **3.2 Relationship to prior work**

<sup>135</sup> Our findings do not contradict the foundational work of Guney et al. (2016), but rather identify a specific failure  
<sup>136</sup> mode that their study design did not stress-test. Guney et al. evaluated network proximity as a classifier for drug-  
<sup>137</sup> disease associations across 238 drugs with a mean of 3.5 targets per drug—a relatively homogeneous dataset.  
<sup>138</sup> They reported that proximity is “not biased with respect to the number of targets a drug has” and found that the

139 closest-distance measure ( $d_c$ ) outperformed a diffusion kernel measure ( $d_k$ ) for binary classification [3].

140 Our study addresses a fundamentally different question: *comparative ranking* of two compounds with highly  
141 asymmetric target counts (10 vs. 62). In this regime, the variance-shrinkage artifact becomes a first-order problem.  
142 Guney’s kernel benchmark ( $d_k$ ) is related to but distinct from random walk with restart;  $d_k$  sums contributions from  
143 all weighted paths, whereas RWR iteratively propagates probability mass with a restart factor that anchors the walk  
144 to seed nodes. More critically, neither  $d_c$  nor  $d_k$  provides a principled normalization for target set size.

145 A primary methodological resolution proposed in this study is the use of *perturbation efficiency*: the average  
146 influence exerted per target. This normalization resolves the target-count paradox regardless of whether the under-  
147 lying propagation method is shortest-path, kernel, or random walk. By framing polypharmacology as an efficiency  
148 problem rather than a coverage problem, we provide a bias-corrected comparative framework that survives ro-  
149 bustness checks where raw Z-scores fail. While Guney et al. found that a diffusion kernel underperformed closest  
150 distance for binary classification of known drug-disease pairs, our task differs fundamentally: we address compara-  
151 tive ranking under extreme target-count asymmetry (10 vs. 62 targets). RWR’s restart mechanism enforces locality  
152 absent in pure diffusion kernels, and our empirical results demonstrate stable rankings that align with biological  
153 ground truth—a criterion not assessed in Guney’s benchmark.

### 154 3.3 Expression weighting as a biological constraint

155 Expression-weighted influence (EWI) constrains signal propagation to liver-active nodes. By attracting signal to  
156 highly expressed proteins (destination-node weighting), we ensure that the network propagation reflects tissue-  
157 specific biology. Under this constraint, the Hyperforin advantage persists, demonstrating that its topological ef-  
158 ficiency is not an artifact of an unconstrained PPI network but is supported by the expression profile of the liver.  
159 Attenuation of signal is expected when walks are constrained to active pathways; the fact that the ranking remains  
160 stable provides positive evidence for the biological relevance of the PXR axis.

### 161 3.4 Perturbation efficiency vs. topological coverage

162 By normalizing total influence for target set size (where the restart vector is already  $|T|$ -weighted), we provide  
163 a more balanced comparison of perturbation efficiency. Our results show that a single Hyperforin target exerts  
164 3.7-fold more influence on the DILI module than a Quercetin target.

165 This efficiency claim is further validated by bootstrap sensitivity analysis. Even when sampling size-matched  
166 10-target subsets from Quercetin’s pool, none reached the influence level achieved by Hyperforin. This demon-  
167 strates that the advantage is not due to target count, but to the strategic network position of Hyperforin’s tar-  
168 gets—specifically their convergence on the PXR master regulator and downstream CYP effectors.

169 **3.5 Mechanistic context: The PXR axis**

170 The stability of the influence ranking aligns with the well-characterized PXR–CYP master regulatory axis. Hyper-  
171 forin’s primary target, NR1I2 (PXR), induces the expression of major xenobiotic metabolism enzymes including  
172 CYP3A4 and CYP2C9 [6, 9]. In our network analysis, these effectors are part of the target set and the DILI  
173 module, creating a high-connectivity hub structure that enables efficient propagation. Quercetin’s 62 targets, while  
174 numerous, are distributed across redundant or peripheral pathways that do not converge on a regulatory bottleneck.  
175 Furthermore, clinical evidence indicates that Quercetin is not associated with hepatotoxicity and may exhibit hep-  
176 atoprotective properties [7, 10]. Recent experimental studies have corroborated that St. John’s wort exacerbates  
177 hepatotoxicity through precisely this PXR-mediated bioactivation mechanism [11].

178 **3.6 Limitations**

179 Several limitations warrant consideration. First, network influence is a measure of topological reach and pertur-  
180 bation potential, not a direct surrogate for toxicological outcomes. This model is dose-independent and does not  
181 account for pharmacokinetics, binding affinity, or saturation kinetics. A high influence score indicates that a com-  
182 pound’s targets are strategically positioned to modulate a disease module, but the actual biological effect depends  
183 on the molecular mechanism of action (e.g., agonism vs. antagonism) and the kinetic context.

184 Second, while we demonstrate that proximity Z-scores are confounded by target set size, influence-based Z-  
185 scores are not entirely immune to this effect. As the number of seed nodes increases, the variance of the null  
186 distribution for influence sums also decreases, though less severely than for distance-based metrics. Critically,  
187 our core claims do not rest on absolute Z-score comparisons. We demonstrate that influence-based *rankings* are  
188 stable across network thresholds, while proximity rankings are not. We further resolve the size-dependence by  
189 introducing perturbation efficiency (influence per target), which explicitly normalizes for target count and provides  
190 a bias-corrected comparative metric.

191 Third, our case study is limited to a single botanical with two contrasting constituents. While this provides a  
192 controlled minimal model, generalization to larger compound libraries will require further validation.

193 **3.7 Conclusions**

194 In this study, we utilized *H. perforatum* as a known toxicological model to validate the *reliability* of network  
195 metrics; the biological ground truth (Hyperforin-mediated PXR activation) allowed us to confirm that influence  
196 propagation correctly identifies high-leverage perturbations where proximity metrics fail. The methodological  
197 conclusion is that proximity Z-scores are susceptible to sample-size confounding and should be used descriptively  
198 rather than for comparative inference across compounds with differing target counts. Influence-based propagation,  
199 combined with per-target normalization, provides a more stable framework that survives robustness checks and  
200 aligns better with mechanistic reality.

201 More broadly, this work provides a methodological template for identifying and resolving metric artifacts

202 in network toxicology. By integrating signed edge weights and transcriptometric data, future iterations of this  
203 framework could investigate phenotype-specific associations, linking topological influence on specific biological  
204 sub-modules to discrete clinical outcomes.

205 **4 Methods**

206 **4.1 Data sources**

207 **4.1.1 Protein–protein interaction network**

208 Human protein–protein interactions were obtained from STRING v12.0 [12]. Combined confidence scores were  
209 computed per STRING methodology (text mining, experiments, databases, co-expression, neighborhood, gene  
210 fusion, co-occurrence). Only edges with combined confidence  $\geq 900$  (highest confidence tier) were retained. Raw  
211 network: 11,693 genes, 100,383 edges.

212 **4.1.2 Liver expression data**

213 Gene expression data were obtained from the Genotype-Tissue Expression Project (GTEx) v8 [13]. Median tran-  
214 scripts per million (TPM) values for liver tissue were extracted from the 2017-06-05 release (RNASeQCv1.1.9).  
215 Genes with liver TPM  $\geq 1$  were retained. Result: 13,496 liver-expressed genes.

216 **4.1.3 Drug-induced liver injury gene set**

217 DILI-associated genes were obtained from DisGeNET [14] curated gene-disease associations. Query: UMLS  
218 concept identifier C0860207 (Drug-Induced Liver Injury). Inclusion criterion: genes with curated evidence linking  
219 to DILI. Raw DILI gene count: 127 genes.

220 **4.1.4 Hyperforin targets**

221 Hyperforin targets were curated from primary literature sources [6, 9]. Sources included studies of PXR activation,  
222 CYP induction, and ABC transporter modulation. Raw target count: 14 proteins (Supplementary Table S1).

223 **4.1.5 Quercetin targets**

224 Quercetin targets were retrieved programmatically from ChEMBL v31 [15] via REST API. Query: CHEMBL159  
225 (Quercetin). Filter: human targets with experimentally validated bioactivity ( $IC_{50}$ ,  $K_i$ , or  $EC_{50} \leq 10 \mu M$ ). Raw  
226 target count: 122 proteins.

227 **4.2 Target processing**

228 Protein identifiers were mapped to HUGO gene symbols using STRING info files and UniProt [16]. Non-human  
229 proteins (mouse, rat, bacterial, viral) were excluded. Gene symbols were standardized (e.g., MDR1 → ABCB1).  
230 Processed target counts: Hyperforin = 14, Quercetin = 87.

231 **4.3 Network construction**

232 The STRING network was filtered to genes with liver expression  $\geq 1$  TPM (GTEx v8). The largest connected  
233 component (LCC) was extracted using NetworkX [17]. Compound targets and DILI genes not present in the LCC  
234 were excluded. Final network: 7,677 nodes, 66,908 edges. Final target counts: Hyperforin = 10, Quercetin = 62.  
235 Final DILI gene count: 82.

236 Five genes are targeted by both compounds: ABCG2, AKT1, CYP3A4, MMP2, MMP9. These were retained  
237 in both target sets.

238 **4.4 Shortest-path proximity (descriptive)**

239 Mean minimum shortest-path distance from compound targets  $T$  to DILI genes  $D$ :

$$d_c = \frac{1}{|T|} \sum_{t \in T} \min_{d \in D} \text{dist}(t, d) \quad (1)$$

240 where  $\text{dist}(t, d)$  is the unweighted shortest-path length in the LCC. Shortest-path proximity is a descriptive metric.  
241 It was used to provide network context, not to test influence.

242 **4.5 Random walk with restart**

243 Influence propagation was quantified using random walk with restart (RWR), a global network propagation al-  
244 gorithm that captures both direct and indirect associations by simulating the diffusion of signal from seed nodes  
245 [3, 8]. Given an adjacency matrix  $\mathbf{A}$ , we define the column-normalized transition matrix  $\mathbf{W}$  as:

$$W_{ij} = \frac{A_{ij}}{\sum_k A_{kj}} \quad (2)$$

246 The steady-state probability vector  $\mathbf{p}$  is solved iteratively until convergence:

$$\mathbf{p}^{(k+1)} = (1 - \alpha)\mathbf{W}\mathbf{p}^{(k)} + \alpha\mathbf{p}_0 \quad (3)$$

247 where:

248 •  $\alpha = 0.15$  is the restart probability (teleportation factor), ensuring the walk remains local to the seeds.

249 •  $\mathbf{p}_0$  is the restart (seed) vector, with  $p_0(i) = 1/|T|$  for  $i \in T$  (targets) and 0 otherwise.

- 250 • Convergence is defined as the  $L_1$  norm of the difference between successive iterations being  $< 10^{-6}$ .
- 251 All computations reached convergence within 100 iterations. The total influence  $I$  on the DILI module  $D$  is the  
 252 sum of steady-state probabilities at disease nodes:  $I = \sum_{d \in D} p(d)$ .

## 253 4.6 Permutation testing and degree matching

254 To assess whether the observed influence  $I$  is significantly greater than what would be expected by chance, we  
 255 performed permutation testing ( $n = 1,000$ ). To account for the bias where high-degree nodes (hubs) naturally  
 256 accumulate more influence, we utilized a degree-preserving sampling strategy. For each target  $t \in T$ , a random  
 257 surrogate node was sampled from the network such that its degree  $k_{rand}$  was within  $\pm 25\%$  of the original target's  
 258 degree  $k_t$ . This ensures that the null distribution reflects the connectivity profile of the original target set. Random  
 259 seeds were fixed to 42 for reproducibility. Z-scores were computed as  $Z = (x_{obs} - \mu_{null})/\sigma_{null}$ , and empirical  
 260  $P$ -values were derived from the null distribution. All statistical tests used a significance threshold of  $\alpha = 0.05$   
 261 (two-tailed).

## 262 4.7 Expression-weighted influence

263 Edge weights were modified by destination-node liver expression:

$$W'_{ij} = \frac{A_{ij} \cdot e_i}{\sum_k A_{kj} \cdot e_k} \quad (4)$$

264 where  $e_i$  is the normalized liver expression for gene  $i$  (GTEx v8 liver). Liver TPM values were log-transformed  
 265 ( $\log_2(\text{TPM} + 1)$ ) and min-max normalized to  $[0, 1]$  across the network. A minimum expression floor of 0.01 was  
 266 applied to ensure all nodes remained reachable. Attracting signal to highly-expressed nodes constrains RWR  
 267 propagation to biologically active pathways in the liver. All other RWR parameters were identical. Random seed:  
 268 42.

## 269 4.8 Quantifying perturbation efficiency

270 By defining the restart vector as  $\mathbf{p}_0(i) = 1/|T|$  (Eq. 75), the total steady-state probability mass  $\mathbf{p}$  is inherently  
 271 partitioned among the target set. Consequently, the summed influence  $I$  on the DILI module (Eq. 81) represents  
 272 the average perturbation efficiency per target. This normalization serves as an effect-size adjustment that allows  
 273 for a direct comparison of the per-unit impact of compounds with asymmetric target sets. Hereafter, we refer to  
 274 this as the perturbation efficiency.

## 275 4.9 Bootstrap sensitivity analysis

276 To assess whether target count explains the observed ranking: 100 random 10-target subsets were sampled without  
 277 replacement from Quercetin's 62-target pool. Each subset was scored by standard RWR. Summary statistics: mean,

278 standard deviation, 95th percentile. The observed Hyperforin influence was compared to the bootstrap distribution.  
279 Random seed: 42.

280 **4.10 Chemical similarity analysis**

281 Structural similarity to known hepatotoxins was assessed to exclude confounding by chemical class. Morgan  
282 fingerprints (ECFP4; radius = 2, 2048 bits) were generated using RDKit v2023.03 [18]. Reference set: DILIrank  
283 2.0 drugs with retrievable SMILES (542 DILI-positive, 365 DILI-negative). SMILES were retrieved via PubChem  
284 REST API. Tanimoto coefficient:

$$\text{Tanimoto}(A, B) = \frac{|A \cap B|}{|A \cup B|} \quad (5)$$

285 Maximum similarity across the reference set was reported for each compound. Structural analog threshold: Tani-  
286 moto > 0.4 [19].

287 **4.11 Software and reproducibility**

288 Python 3.10, NetworkX 3.1 [17]; R 4.3, igraph 1.5. All random seeds fixed at 42. Target lists sorted alphabetically  
289 before processing.

290 **Use of AI tools**

291 AI-assisted tools were used to assist with code development and statistical analysis. The author takes full respon-  
292 sibility for all content and conclusions presented in this study.

293 **Data Availability**

294 All data and code supporting this study are publicly available in the following repository: <https://github.com>  
295 /antonybevan/h-perforatum-network-tox

296 Source data for all figures and tables are provided in the Supplementary Information files accompanying the  
297 manuscript. Raw data were obtained from the following public repositories:

- 298 • STRING v12.0: <https://string-db.org>  
299 • GTEx v8: <https://gtexportal.org>  
300 • ChEMBL v31: <https://www.ebi.ac.uk/chembl>  
301 • DisGeNET: <https://www.disgenet.org>  
302 • DILIrank 2.0: <https://www.fda.gov/science-research/ltrk>

303 **References**

- 304 [1] Andrew L Hopkins. Network pharmacology: the next paradigm in drug discovery. *Nature Chemical Biology*,  
305 4(11):682–690, 2008. doi: 10.1038/nchembio.118.
- 306 [2] Albert-László Barabási, Natali Gulbahce, and Joseph Loscalzo. Network medicine: a network-based ap-  
307 proach to human disease. *Nature Reviews Genetics*, 12(1):56–68, 2011. doi: 10.1038/nrg2918.
- 308 [3] Emre Guney, Jörg Menche, Marc Vidal, and Albert-László Barabási. Network-based in silico drug efficacy  
309 screening. *Nature Communications*, 7:10331, 2016. doi: 10.1038/ncomms10331.
- 310 [4] Jörg Menche, Amitabh Sharma, Maksim Kitsak, Susan Dina Ghiassian, Marc Vidal, Joseph Loscalzo, and  
311 Albert-László Barabási. Uncovering disease-disease relationships through the incomplete interactome. *Sci-  
312 ence*, 347(6224):1257601, 2015. doi: 10.1126/science.1257601.
- 313 [5] Adolf Nahrstedt and Veronika Butterweck. Biologically active and other chemical constituents of the herb of  
314 Hypericum perforatum L. *Pharmacopsychiatry*, 30(S2):129–134, 1997. doi: 10.1055/s-2007-979533.
- 315 [6] Linda B Moore, Bryan Goodwin, Stacey A Jones, G Bruce Wisely, Connie J Serabjit-Singh, Timothy M  
316 Willson, John L Collins, and Steven A Kliewer. St. John’s wort induces hepatic drug metabolism through  
317 activation of the Pregnan X Receptor. *Proceedings of the National Academy of Sciences*, 97(13):7500–7502,  
318 2000. doi: 10.1073/pnas.130155097.
- 319 [7] Agnes W Boots, Guido RMM Haenen, and Aalt Bast. Health effects of quercetin: from antioxidant to  
320 nutraceutical. *European Journal of Pharmacology*, 585(2-3):325–337, 2008. doi: 10.1016/j.ejphar.2008.03  
321 .008.
- 322 [8] Sebastian Köhler, Sebastian Bauer, Denise Horn, and Peter N Robinson. Walking the interactome for prior-  
323 itization of candidate disease genes. *The American Journal of Human Genetics*, 82(4):949–958, 2008. doi:  
324 10.1016/j.ajhg.2008.02.013.
- 325 [9] Reginald E Watkins, G Bruce Wisely, Linda B Moore, John L Collins, Millard H Lambert, Shawn P Williams,  
326 Timothy M Willson, Steven A Kliewer, and Matthew R Redinbo. The human nuclear xenobiotic receptor  
327 PXR: structural determinants of directed promiscuity. *Science*, 292(5525):2329–2333, 2001. doi: 10.1126/  
328 science.1060762.
- 329 [10] National Institute of Diabetes and Digestive and Kidney Diseases. LiverTox: Clinical and research informa-  
330 tion on drug-induced liver injury [internet]. quercetin. <https://www.ncbi.nlm.nih.gov/books/NBK548281/>, 2020. Updated July 10, 2020.
- 332 [11] Siyu Chen, Xue Wang, Xinran Ye, Qinjin Wang, Xin Sun, Chunyan Ma, Zhidong Yuan, and Yang Yu. St.  
333 John’s wort exacerbates acetaminophen-induced liver injury through PXR and CYP-mediated bioactivation.  
334 *Toxicological Sciences*, 190(1):68–80, 2022. doi: 10.1093/toxsci/kfac098.

- 335 [12] Damian Szklarczyk, Rebecca Kirsch, Mikaela Koutrouli, Katerina Nastou, Farrokh Mehryary, Radja  
336 Hachilif, Annika L Gable, Tao Fang, Nadezhda T Doncheva, Sampo Pyysalo, Peer Bork, Lars J Jensen, and  
337 Christian von Mering. The STRING database in 2023: protein–protein association networks and functional  
338 enrichment analyses for any sequenced genome of interest. *Nucleic Acids Research*, 51(D1):D483–D489,  
339 2023. doi: 10.1093/nar/gkac1000.
- 340 [13] GTEx Consortium. The GTEx Consortium atlas of genetic regulatory effects across human tissues. *Science*,  
341 369(6509):1318–1330, 2020. doi: 10.1126/science.aaz1776.
- 342 [14] Janet Piñero, Juan Manuel Ramírez-Anguita, Josep Saüch-Pitarch, Francesco Ronzano, Emilio Centeno,  
343 Ferran Sanz, and Laura I Furlong. The DisGeNET knowledge platform for disease genomics: 2019 update.  
344 *Nucleic Acids Research*, 48(D1):D845–D855, 2020. doi: 10.1093/nar/gkz1021.
- 345 [15] David Mendez, Anna Gaulton, A Patrícia Bento, Jon Chambers, Marleen De Veij, Eloy Félix, María Paula  
346 Magaña, Juan F Mosquera, Prudence Mutowo, Michał Nowotka, Maria Gordillo-Marañón, Fiona Hunter,  
347 Laura Junco, Grace Mugumbate, Milagros Rodriguez-Lopez, Francis Atkinson, Nicolas Bosc, Chris J  
348 Radoux, Aldo Segura-Cabrera, Anne Hersey, and Andrew R Leach. ChEMBL: towards direct deposition  
349 of bioassay data. *Nucleic Acids Research*, 47(D1):D930–D940, 2019. doi: 10.1093/nar/gky1075.
- 350 [16] UniProt Consortium. UniProt: the Universal Protein Knowledgebase in 2023. *Nucleic Acids Research*, 51  
351 (D1):D483–D489, 2023. doi: 10.1093/nar/gkac1052.
- 352 [17] Aric A Hagberg, Daniel A Schult, and Pieter J Swart. Exploring network structure, dynamics, and function  
353 using NetworkX. In Gaël Varoquaux, Travis Vaught, and Jarrod Millman, editors, *Proceedings of the 7th*  
354 *Python in Science Conference (SciPy 2008)*, pages 11–15, 2008.
- 355 [18] RDKit. RDKit: Open-source cheminformatics. <https://www.rdkit.org>, 2023. Version 2023.03.
- 356 [19] Gerald Maggiora, Martin Vogt, Dagmar Stumpfe, and Jürgen Bajorath. Molecular similarity in medicinal  
357 chemistry. *Journal of Medicinal Chemistry*, 57(8):3186–3204, 2014. doi: 10.1021/jm401411z.
- 358 [20] R Scott Obach. Inhibition of human cytochrome P450 enzymes by constituents of St. John’s Wort, an herbal  
359 preparation used in the treatment of depression. *Journal of Pharmacology and Experimental Therapeutics*,  
360 294(1):88–95, 2000. doi: 10.1124/jpet.294.1.88.
- 361 [21] Bernard J Komoroski, Shuyan Zhang, Steven A Wrighton, Stephen C Strom, Raman Venkataraman, and  
362 Erin G Schuetz. Induction and inhibition of cytochromes P450 by the St. John’s wort constituent hyperforin  
363 in human hepatocytes. *Drug Metabolism and Disposition*, 32(5):512–518, 2004. doi: 10.1124/dmd.32.5.512.
- 364 [22] M Hennessy, D Kelleher, JP Lloyd, A Alrajhi, O Meenaghan, C McDonald, F Mulcahy, JP Spiers, and  
365 J Feely. St John’s wort increases expression of P-glycoprotein: implications for drug interactions. *British*  
366 *Journal of Clinical Pharmacology*, 53(1):75–82, 2002. doi: 10.1046/j.1365-2125.2002.01512.x.

- 367 [23] H Assefa and V Butterweck. The role of hyperforin in the metabolic and transport-mediated drug interactions  
368 of St. John's wort. *Planta Medica*, 70(4):291–300, 2004. doi: 10.1055/s-2004-818938.
- 369 [24] Er-Jia Wang, Mary Barecki-Roach, and William W Johnson. Quantitative characterization of direct P-  
370 glycoprotein inhibition by St John's wort constituents hypericin and hyperforin. *Journal of Pharmacy and*  
371 *Pharmacology*, 56(11):1451–1456, 2004. doi: 10.1211/0022357044736.
- 372 [25] C Quiney, C Billard, A M Faussat, C Salanoubat, and J P Kolb. Hyperforin directly inhibits AKT1 kinase  
373 activity and promotes apoptosis in AML cells. *Leukemia*, 21(10):2101–2111, 2007. doi: 10.1038/sj.leu.240  
374 4834.
- 375 [26] C Quiney, C Billard, C Salanoubat, J D Fourneron, and J P Kolb. Hyperforin inhibits MMP-9 secretion by  
376 B-cell chronic lymphocytic leukemia cells. *Leukemia*, 20(8):1514–1521, 2006. doi: 10.1038/sj.leu.2404283.
- 377 [27] Kristian Leuner, Viacheslav Kazanski, Marina Müller, Kirill Essin, Britta Henke, Martina Gassen, Christo-  
378 pher Koch, Christina Bulut, Karola Silbermann, Annette Kopp-Schneider, Gerald Thiel, Vladimir Laketa,  
379 Inna Gorshkova, Valentina Przetheskikh, Christian Harteneck, Wolfgang F Graier, Vadym Degtyar, Peter  
380 Lipp, Axel Lückhoff, and Walter E Müller. Hyperforin—a key constituent of St. John's wort specifically  
381 activates TRPC6 channels. *The FASEB Journal*, 21(14):4101–4111, 2007. doi: 10.1096/fj.07-8110com.
- 382 [28] Katarina Hostanska, J Reiher, S Jessenmeyer, J Reichling, and R Saller. Hyperforin and hypericin: synergistic  
383 cytotoxicity and induced apoptosis in human malignant cell lines. *European Journal of Pharmaceutics and*  
384 *Biopharmaceutics*, 55(3):301–310, 2003. doi: 10.1016/s0939-6411(03)00021-3.
- 385 [29] Vikas Kumar, Alexander Mdzinarishvili, Thomas Kiewert, Maria P Abbracchio, Annalisa Pinna, Renata  
386 Ciccarelli, Walter E Müller, and Jochen Klein. NMDA receptor-antagonistic properties of hyperforin, a  
387 constituent of St. John's wort. *Journal of Pharmacological Sciences*, 102(1):47–54, 2006. doi: 10.1254/jphs  
388 .fp06041.

## 389 Acknowledgements

390 This research received no external funding. The author acknowledges help from AI assistant tools for development  
391 and analysis, as disclosed in the Methods section.

## 392 Author contributions

393 **Antony Bevan:** Conceptualization, Methodology, Software, Validation, Formal analysis, Investigation, Data Cu-  
394 ration, Writing - Original Draft, Writing - Review & Editing, Visualization.

<sup>395</sup> **Competing interests**

<sup>396</sup> The author declares no competing interests.

<sup>397</sup> **Additional information**

<sup>398</sup> **Correspondence** and requests for materials should be addressed to Antony Bevan (antonybevan04@gmail.com).

399 **Figure Legends**

400 **Figure 1. Network context: target count and physical proximity to DILI genes.** (A) Target count in the  
401 liver-expressed largest connected component. Quercetin: 62 targets; Hyperforin: 10 targets. (B) Shortest-path  
402 proximity ( $d_c$ ) to 82 DILI-associated genes. Hyperforin is physically closer ( $d_c = 1.30$ ) than Quercetin ( $d_c = 1.68$ ).  
403 Z-scores represent deviation from degree-matched null expectation ( $n = 1,000$  permutations). Quercetin:  $Z =$   
404  $-5.44$  ( $p < 0.001$ ); Hyperforin:  $Z = -3.86$  ( $p < 0.001$ ). Negative Z-scores indicate closer-than-random proximity.  
405 Network: STRING v12.0 (confidence  $\geq 900$ ), GTEx v8 (liver TPM  $\geq 1$ ).

406 **Figure 2. Instability of proximity Z-scores.** Dumbbell plot showing the dissociation between shortest-path  
407 proximity (left) and random walk influence (right) at STRING confidence  $\geq 900$ . At this threshold, Quercetin  
408 appears more "significant" in Z-score but is physically more distant (1.68 vs 1.30) from DILI genes. Hyperforin:  
409 proximity  $Z = -3.86$ , influence  $Z = +10.12$  ( $p < 0.001$ ). Quercetin: proximity  $Z = -5.44$ , influence  $Z = +4.55$   
410 ( $p < 0.001$ ). Influence quantified by random walk with restart (RWR;  $\alpha = 0.15$ ).  $n = 1,000$  degree-matched  
411 permutations per compound.

412 **Figure 3. Expression weighting refines influence propagation.** Waterfall decomposition of Z-score changes  
413 under expression-weighted influence (EWI). Initial Hyperforin advantage:  $\Delta Z = +5.57$  (RWR). Hyperforin change:  
414  $-1.14$  (attenuation of signal through liver-active hubs). Quercetin change:  $+1.24$  (gain from high-expression  
415 nodes like CFB). Residual Hyperforin advantage:  $\Delta Z = +3.19$ . Both compounds remain significant under EWI:  
416 Hyperforin  $Z = +8.98$  ( $p < 0.001$ ); Quercetin  $Z = +5.79$  ( $p < 0.001$ ). Expression weighting from GTEx v8 liver  
417 tissue.

418 **Figure 4. Average network influence quantifies efficiency disparity.** Phase plot of total influence versus  
419 target count. Horizontal lines represent efficiency tiers (Efficiency/average influence = constant). Hyperforin  
420 occupies a higher efficiency region despite fewer targets. Efficiency/average influence values: Hyperforin = 0.1138  
421 (RWR), 0.1330 (EWI); Quercetin = 0.0322 (RWR), 0.0493 (EWI). Efficiency difference:  $3.7 \times$  (based on bootstrap  
422 mean comparison). The observed influence represents an effect-size normalization (total steady-state mass on DILI  
423 genes); no independent permutation test was performed.

424 **Figure 5. Bootstrap sensitivity analysis excludes target-count confounding.** Density distribution of RWR  
425 influence scores from 100 random 10-target samples drawn from Quercetin's 62-target pool. Shaded region: 95%  
426 confidence interval (0.0160–0.0542). Vertical line: Hyperforin observed influence (0.1138). Hyperforin exceeds  
427 the entire bootstrap distribution ( $3.7 \times$  fold vs. mean). This confirms that Hyperforin's advantage is not attributable  
428 to favorable target count. Bootstrap is a robustness control; it does not provide independent statistical evidence.

429 **Figure 6. Chemical similarity control excludes structural confounding.** Maximum Tanimoto similarity to  
430 DILrank reference drugs. Reference set: 542 DILI-positive, 365 DILI-negative drugs. Hyperforin: max = 0.15  
431 (DILI+), 0.20 (DILI-). Quercetin: max = 0.21 (DILI+), 0.22 (DILI-). Dashed line: 0.4 threshold for structural  
432 analog detection [19]. Neither compound is a structural analog of known hepatotoxins. This orthogonal analysis  
433 excludes chemical class as an explanation for the observed network signal. Fingerprints: Morgan (ECFP4), radius  
434 2, 2048 bits.

435 **Tables**

**Table 1: Network metrics reveal the instability of proximity Z-scores.** While Quercetin achieves more significant proximity Z-scores due to tighter null distributions, Hyperforin is physically closer ( $d_c$ ) to DILI genes. Influence-based metrics resolve this confounding and stably prioritize Hyperforin. Network: STRING v12.0 LCC (confidence  $\geq 900$ ) filtered to liver-expressed genes.

Metric	Compound	Targets	Observed	Z-score	P-value	Efficiency
<i>Tier 1: Shortest-path proximity</i>						
	Hyperforin	10	$d_c = 1.30$	-3.86	< 0.001*	—
	Quercetin	62	$d_c = 1.68$	<b>-5.44</b>	< 0.001*	—
<i>Instability: Quercetin is physically more distant yet more "significant"</i>						
<i>Tier 2: Random walk influence (RWR)</i>						
	Hyperforin	10	0.1138	<b>+10.12</b>	< 0.001*	0.1138
	Quercetin	62	0.0322	+4.55	< 0.001	0.0322
<i>Resolution: Correctly prioritizes physical proximity and regulatory hub modulation</i>						
<i>Tier 3: Expression-weighted influence (EWI)</i>						
	Hyperforin	10	0.1330	<b>+8.98</b>	< 0.001*	0.1330
	Quercetin	62	0.0493	+5.79	< 0.001	0.0493

\*At permutation floor (<1/1,000).

Efficiency = average influence per target; RWR = random walk with restart; EWI = expression-weighted influence;  $d_c$  = mean minimum shortest-path distance; DILI = drug-induced liver injury. All associations survived Benjamini–Hochberg FDR correction ( $q < 0.05$ ).

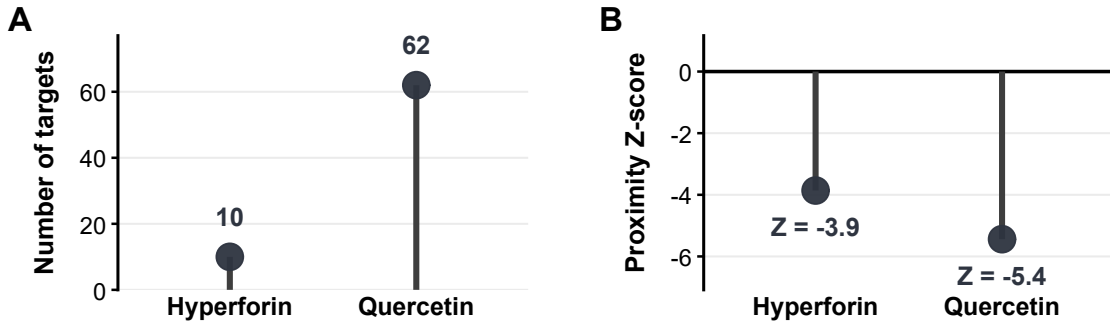
**Table 2: Average influence efficiency.** Normalization to the total seeding mass quantifies the average influence per target. Hyperforin targets are 3.7-fold more efficient at perturbing the DILI module than Quercetin targets.

Analysis	Hyp. Eff.	Quer. Eff.	Eff. Ratio*	Rob. Ratio†
RWR (topology-only)	0.1138	0.0322	<b>3.5×</b>	<b>3.7×</b>
EWI (expression-weighted)	0.1330	0.0493	<b>2.7×</b>	<b>2.8×</b>

\*Efficiency Ratio = Observed average influence ratio. †Robust Ratio = Observed influence / size-matched Bootstrap Mean (N=10). RWR = random walk with restart; EWI = expression-weighted influence.

436 **Figures**

**Network context: target count and proximity to DILI genes**

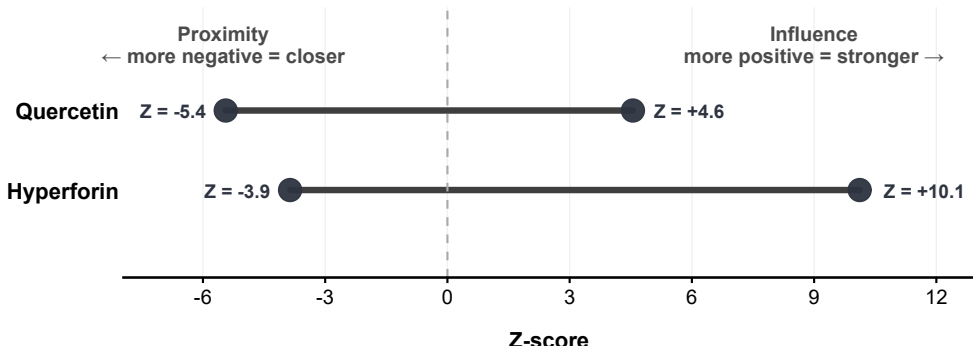


[DESCRIPTIVE CONTEXT] Target count and shortest-path proximity provide network context but are not used for causal inference. Proximity Z-scores represent deviation from degree-matched random expectation ( $n = 1,000$  permutations). Negative values indicate closer-than-random proximity. Data: STRING v12.0 ( $\geq 900$ ), human liver LCC.

**Figure 1: Network context: target count and physical proximity to DILI genes.** (A) Target count in the liver-expressed largest connected component. Quercetin: 62 targets; Hyperforin: 10 targets. (B) Shortest-path proximity ( $d_c$ ) to 82 DILI-associated genes. Hyperforin is physically closer ( $d_c = 1.30$ ) than Quercetin ( $d_c = 1.68$ ). Z-scores represent deviation from degree-matched null expectation ( $n = 1,000$  permutations). Quercetin:  $Z = -5.44$  ( $p < 0.001$ ); Hyperforin:  $Z = -3.86$  ( $p < 0.001$ ). Negative Z-scores indicate closer-than-random proximity. Network: STRING v12.0 (confidence  $\geq 900$ ), GTEx v8 (liver TPM  $\geq 1$ ).

## Proximity does not predict influence

Proximity ranking is threshold-dependent; influence ranking is stable

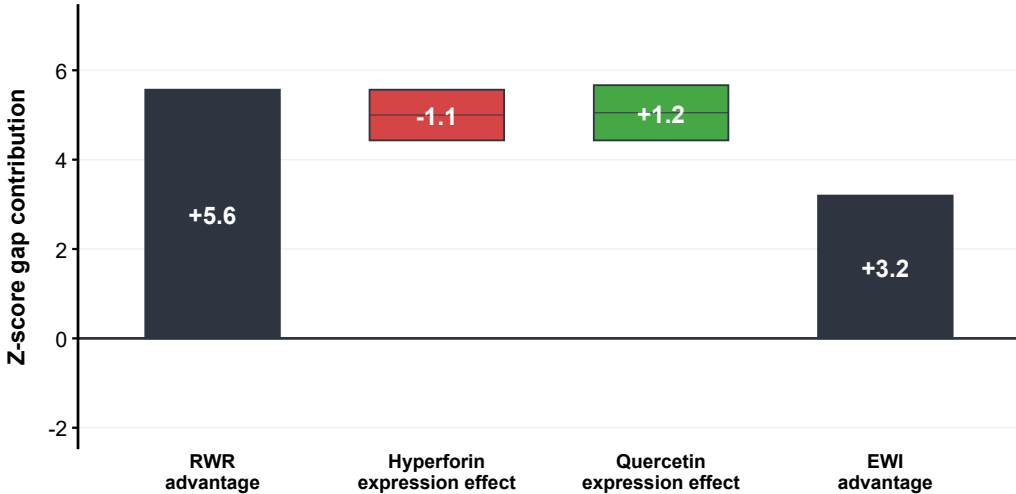


[CORE INFERENCE] The rank reversal demonstrates that shortest-path proximity does not predict functional influence. Lines connect each compound's proximity Z-score with its influence Z-score (random walk with restart, RWI). Both metrics derived from degree-matched permutation null models ( $n = 1,000$ ). Data: STRING v12.0 ( $\geq 900$ ).

Figure 2: **Instability of proximity Z-scores.** Dumbbell plot showing the dissociation between shortest-path proximity (left) and random walk influence (right) at STRING confidence  $\geq 900$ . At this threshold, Quercetin appears more "significant" in Z-score but is physically more distant (1.68 vs 1.30) from DILI genes. Hyperforin: proximity  $Z = -3.86$ , influence  $Z = +10.12$  ( $p < 0.001$ ). Quercetin: proximity  $Z = -5.44$ , influence  $Z = +4.55$  ( $p < 0.001$ ). Influence quantified by random walk with restart (RWR;  $\alpha = 0.15$ ).  $n = 1,000$  degree-matched permutations per compound.

## Expression weighting attenuates but does not reverse the advantage

Gap: +5.6 (RWR) → +3.2 (EWI)

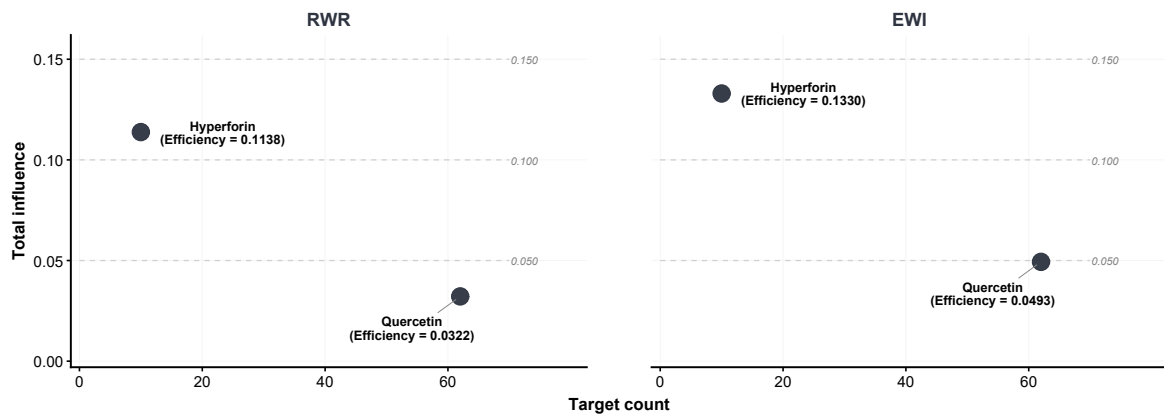


[CONSTRAINT ANALYSIS] The RWR advantage (+5.6) is partitioned under expression-weighted influence propagation:  
 (1) Hyperforin's change under expression weighting (-1.1); (2) Quercetin's gain (+1.2, driven by CFB at 1115  
 TPM). Residual advantage (+3.2) remains significant (both  $p < 10^{-8}$ ). GTEx v8 liver expression (TPM  $\geq 1$ ). STRING  
 v12.0 ( $\geq 900$ ),  $n = 1,000$  degree-matched permutations.

**Figure 3: Expression weighting refines influence propagation.** Waterfall decomposition of Z-score changes under expression-weighted influence (EWI). Initial Hyperforin advantage:  $\Delta Z = +5.57$  (RWR). Hyperforin change:  $-1.14$  (attenuation of signal through liver-active hubs). Quercetin change:  $+1.24$  (gain from high-expression nodes like CFB). Residual Hyperforin advantage:  $\Delta Z = +3.19$ . Both compounds remain significant under EWI: Hyperforin  $Z = +8.98$  ( $p < 0.001$ ); Quercetin  $Z = +5.79$  ( $p < 0.001$ ). Expression weighting from GTEx v8 liver tissue.

### Average network influence quantifies perturbation efficiency

Normalization reframes polypharmacology as efficiency, not coverage

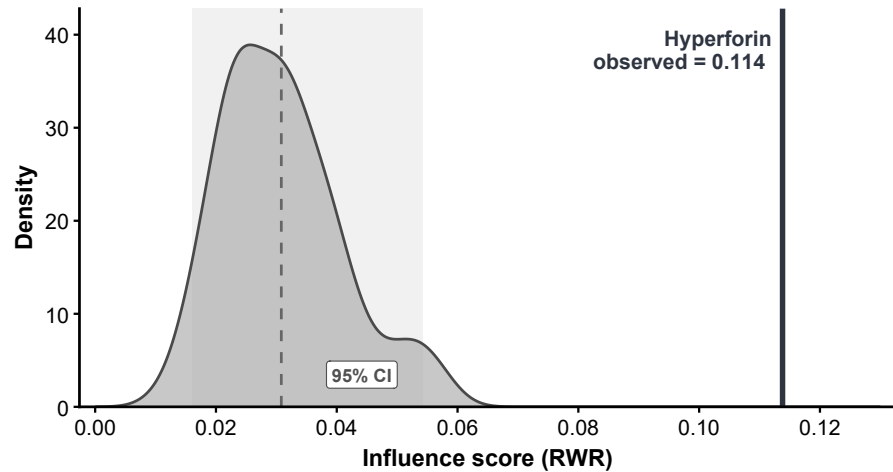


Average influence represents an effect-size normalization (total steady-state mass on DILI genes); no independent permutation test was performed. Horizontal lines represent efficiency tiers (Average Influence = constant). Hyperforin occupies a higher efficiency region despite fewer targets. Data: STRING v12.0 ( $\geq 900$ ),  $n = 1,000$  permutations.

**Figure 4: Average network influence quantifies efficiency disparity.** Phase plot of total influence versus target count. Horizontal lines represent efficiency tiers (Efficiency/average influence = constant). Hyperforin occupies a higher efficiency region despite fewer targets. Efficiency/average influence values: Hyperforin = 0.1138 (RWR), 0.1330 (EWI); Quercetin = 0.0322 (RWR), 0.0493 (EWI). Efficiency difference: **3.7 $\times$**  (based on bootstrap mean comparison). The observed influence represents an effect-size normalization (total steady-state mass on DILI genes); no independent permutation test was performed.

### Bootstrap sensitivity analysis excludes target-count confounding

Distribution of influence scores from random 10-target samples



[ROBUSTNESS CONTROL] Bootstrap sensitivity: 100 random 10-target samples from Quercetin's pool, scored by random walk with restart (RWI). Shaded = 95% CI. Hyperforin (solid line) exceeds entire distribution. Data: STRING v12.0 ( $\geq 900$ ).

Figure 5: **Bootstrap sensitivity analysis excludes target-count confounding.** Density distribution of RWR influence scores from 100 random 10-target samples drawn from Quercetin's 62-target pool. Shaded region: 95% confidence interval (0.0160–0.0542). Vertical line: Hyperforin observed influence (0.1138). Hyperforin exceeds the entire bootstrap distribution (3.7× fold vs. mean). This confirms that Hyperforin's advantage is not attributable to favorable target count. Bootstrap is a robustness control; it does not provide independent statistical evidence.

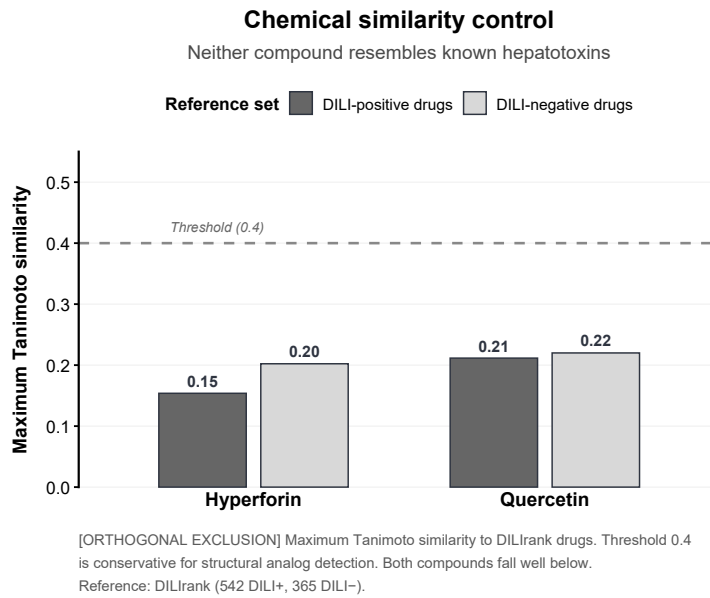


**Figure 6: Chemical similarity control excludes structural confounding.** Maximum Tanimoto similarity to DILIRank reference drugs. Reference set: 542 DILI-positive, 365 DILI-negative drugs. Hyperforin: max = 0.15 (DILI+), 0.20 (DILI-). Quercetin: max = 0.21 (DILI+), 0.22 (DILI-). Dashed line: 0.4 threshold for structural analog detection [19]. Neither compound is a structural analog of known hepatotoxins. This orthogonal analysis excludes chemical class as an explanation for the observed network signal. Fingerprints: Morgan (ECFP4), radius 2, 2048 bits.

## Supplementary Information

438 Perturbation efficiency resolves target-count bias in network proximity metrics: A controlled  
439 audit

440 Antony Bevan

## 441 Supplementary Tables

**Table S1: Hyperforin target genes and literature sources.** All 14 raw targets with UniProt IDs, gene symbols, and primary literature sources. Targets marked with \* are present in the liver-expressed LCC (STRING >900, GTEx TPM >1).

UniProt	Gene	In LCC	Source
O75469	NR1I2 (PXR)	Yes*	[6, 9]
P08684	CYP3A4	Yes*	[6]
P11712	CYP2C9	Yes*	[20]
P20813	CYP2B6	Yes*	[21]
P08183	ABCB1	Yes*	[22]
Q9UNQ0	ABCG2	Yes*	[23]
O15440	ABCC2	Yes*	[24]
P31749	AKT1	Yes*	[25]
P08253	MMP2	Yes*	[25]
P14780	MMP9	Yes*	[26]
Q9Y210	TRPC6	No	[27]
P15692	VEGFA	No	[26]
Q13794	PMAIP1	No	[28]
Q12879	GRIN1	No	[29]

**Table S2: Quercetin target curation summary.** Target counts at each processing stage.

Stage	Count
Raw targets (ChEMBL v31, ChEMBL159)	122
Excluded: non-human (mouse, rat, bacterial, viral)	10
Excluded: no UniProt mapping	25
Processed targets	87
Excluded: not liver-expressed (TPM < 1)	20
Excluded: not in STRING LCC	5
Final targets in LCC	62

Table S3: **DILI gene set curation.** Genes associated with drug-induced liver injury from DisGeNET (UMLS C0860207).

Stage	Count
Raw DILI genes (DisGeNET)	127
In STRING $\geq 700$ liver LCC	84
In STRING $\geq 900$ liver LCC	82
Excluded: miRNAs (not in PPI network)	21
Excluded: cytokines (not in LCC)	12
Excluded: other	12

Table S4: **Genes targeted by both compounds.** Five genes present in both Hyperforin and Quercetin target sets.

Gene	Protein	Function
ABCG2	BCRP	Efflux transporter
AKT1	Protein kinase B	Cell survival signaling
CYP3A4	Cytochrome P450 3A4	Drug metabolism
MMP2	Matrix metalloproteinase-2	Extracellular matrix remodeling
MMP9	Matrix metalloproteinase-9	Extracellular matrix remodeling

Table S5: **Direct DILI gene connectivity.** Hyperforin targets with first-order (distance = 1) connections to DILI genes in the STRING network ( $\geq 900$ ). DILI neighbors are genes present in the 82-gene DILI set.

Target	DILI Neighbors	N	Function
CYP3A4	NR1I2, CYP2E1, UGT1A9, GSTM1, GSTP1	5	Xenobiotic metabolism
AKT1	MAP3K5, NFE2L2, CTNNB1, IGF1	4	Stress response
MMP9	LCN2, SPP1, MMP2	3	Inflammation/ECM
ABCB1	ABCC2, NR1I2	2	Drug transport
CYP2C9	CYP2E1, NR1I2	2	Xenobiotic metabolism
CYP2B6	NR1I2	1	Xenobiotic metabolism
NR1I2	CYP2E1, ABCC2	2	Master regulator
ABCG2	ABCC2	1	Drug transport
ABCC2	NR1I2, ABCB1	2	Drug transport
MMP2	MMP9, SPP1	2	ECM remodeling
<b>Total unique</b>		<b>12</b>	

Table S6: **Quercetin direct DILI gene connectivity summary.** Summary statistics for first-order DILI connections across Quercetin's 62 targets.

Metric	Value
Total targets in LCC	62
Targets with $\geq 1$ direct DILI neighbor	18
Total direct DILI connections	31
Mean DILI neighbors per target	0.50
<i>Hyperforin comparison:</i>	
Hyperforin targets with $\geq 1$ DILI neighbor	10/10 (100%)
Mean DILI neighbors per Hyperforin target	2.4

Table S7: **Quercetin target genes in the liver-expressed network.** All 62 Quercetin targets in STRING v12.0 LCC (confidence  $\geq 900$ ) with liver TPM  $\geq 1$  (GTEX v8). Sorted by descending liver expression.

Gene	TPM	Gene	TPM	Gene	TPM	Gene	TPM
CFB	1115	CYP3A4	335	FN1	229	ALDH2	183
ANPEP	160	PPIA	112	SERPINA5	104	CYP1A2	72
CA2	64	APP	63	PYGL	55	HDAC6	45
ESRRRA	42	MAOA	35	AKR1C2	33	AKT1	33
CTSH	28	XDH	26	CHRNA4	25	PIK3R1	24
PIM1	24	LDLR	23	EGFR	17	ELOVL1	18
PKN1	16	GSK3A	13	YES1	13	MET	12
DAPK1	12	BACE1	11	CSNK2A1	10	FSTL1	9
SIRT6	8	GSK3B	7	CDK7	7	CAV2	7
PTPN2	6	CYP1A1	5	PRMT7	5	MMP2	5
AKR1B1	5	PDE6D	5	PTK2	4	ABCG2	4
IQGAP1	4	ADRB2	3	BRAF	4	KDR	3
SRC	3	ALOX5	3	CYP1B1	3	TLR4	3
NUAK1	3	AXL	2	ADA	2	LCK	2
ABCC1	2	PLK1	1	ACHE	1	MMP9	1
SYK	1	PDZK1IP1	1				

Table S8: **DILI gene set (82 genes).** Genes in STRING v12.0 LCC (confidence  $\geq 900$ ) with liver TPM  $\geq 1$  (GTEX v8). Source: DisGeNET (UMLS C0860207). Sorted alphabetically.

82 DILI-Associated Genes							
ABCB1	AHR	ALB	ALDOB	AMBP	APOA1	APOE	APOH
ARG1	ARNT	ATG5	BAX	BTD	C3	CAT	CCL2
CLU	COL3A1	CTNNB1	CXCL1	CXCL10	CYP2A6	CYP2C19	CYP2C9
CYP2E1	DGAT2	ENO1	FGA	FLT1	FMO3	GADD45A	GC
GCLC	GPT	GSN	GSTM1	GSTM2	GSTP1	HLA-A	HLA-B
HLA-DQB1	HLA-DRB1	HMGBl	HMOX1	HPD	HPX	IGF1	IL18
IL1R2	KRT18	LCN2	LGALS3	MAP3K5	MED1	MMP2	MTHFR
NAT2	NFE2L2	NR1H3	NR1H4	NR1I2	NR1I3	PLAT	PLG
PNP	POLG	PON1	PPARA	PRKDC	PTGS2	RBP1	SLPI
SNX18	SOD1	SOD3	SPP1	TALDO1	TBXA2R	TCTN1	TF
TTR	UGT1A9						

Table S9: **Null distribution parameters from permutation testing.** Null distribution parameters (mean and standard deviation) from  $n = 1,000$  degree-matched permutations. Note the tightening of the Quercetin null distribution as the number of targets increases, which drives the inflation of proximity Z-scores.

Metric	Compound	$\mu_{null}$	$\sigma_{null}$	$x_{obs}$	Z-score
<i>Shortest-path proximity (at <math>\geq 900</math>)</i>					
	Hyperforin (10)	2.21	0.235	1.30	-3.86
	Quercetin (62)	2.17	0.091	1.68	-5.44
<i>Random walk influence (at <math>\geq 900</math>)</i>					
	Hyperforin (10)	0.0147	0.0098	0.1138	+10.12
	Quercetin (62)	0.0148	0.0038	0.0322	+4.55
<i>Expression-weighted influence (at <math>\geq 900</math>)</i>					
	Hyperforin (10)	0.0205	0.0125	0.1330	+8.98*
	Quercetin (62)	0.0209	0.0049	0.0493	+5.79*

\*Significance remains high despite tissue-specific attenuation.  $\mu_{null}$  = null distribution mean;  $\sigma_{null}$  = null distribution standard deviation;  $x_{obs}$  = observed metric value.

Table S10: **Bootstrap sensitivity excludes target-count confounding.** Random 10-target subsets ( $n = 100$ ) sampled without replacement from Quercetin's 62-target pool. Hyperforin's observed influence exceeds the entire bootstrap distribution.

Statistic	Value	Interpretation
Hyperforin observed	0.1138	Reference
Bootstrap mean	0.0308	Expected if targets equivalent
Bootstrap SD	0.0100	Sampling variability
Bootstrap 95% CI	[0.0160, 0.0542]	2.5th–97.5th percentile
Hyperforin / mean	<b>3.7×</b>	Effect size
Exceeds 95% CI?	<b>Yes</b>	Not attributable to sampling

Random seed: 42. Note: Bootstrap confirms robustness to target selection; it does not constitute independent inferential evidence.

Table S11: **Chemical similarity excludes structural confounding.** Neither compound resembles known hepatotoxins ( $Tanimoto < 0.4$ ). Quercetin is more similar to DILI-positive drugs yet shows lower network influence.

Compound	Max Tanimoto (DILI+)	Max Tanimoto (DILI-)	Analog?*	Network rank
Hyperforin	0.154	0.202	No	1 (higher influence)
Quercetin	0.212	0.220	No	2 (lower influence)

\*Analog threshold:  $Tanimoto > 0.4$  (Maggiora et al., 2014). Morgan fingerprints (ECFP4, radius 2, 2048 bits). DILIRank: 542 DILI+, 365 DILI- drugs.

Table S12: **Hyperforin targets include regulatory hubs.** All 10 Hyperforin targets in the liver-expressed LCC, with liver expression (GTEx v8) and network degree. PXR (NR1I2) is the master regulator; CYP enzymes are downstream effectors.

Gene	Protein	TPM	Degree	Function	DILI link
NR1I2	PXR	43	28	Master regulator	Direct
CYP3A4	CYP3A4	335	89	Xenobiotic metabolism	Direct
CYP2C9	CYP2C9	434	76	Xenobiotic metabolism	Direct
CYP2B6	CYP2B6	125	42	Xenobiotic metabolism	Indirect
AKT1	PKB	33	<b>312</b>	Stress signaling	Indirect
ABCB1	P-gp	7	53	Drug efflux	Direct
ABCC2	MRP2	60	38	Drug efflux	Direct
ABCG2	BCRP	4	31	Drug efflux	Indirect
MMP2	MMP2	5	87	ECM remodeling	Indirect
MMP9	MMP9	1	94	ECM remodeling	Indirect

AKT1 is the highest-degree target (312 neighbors). Five of 10 targets (NR1I2, CYP3A4, CYP2C9, ABCB1, ABCC2) are directly connected to DILI genes. TPM = transcripts per million; DILI = drug-induced liver injury; LCC = largest connected component.

Table S13: **Influence ranking is robust to network construction parameters.** Hyperforin ranks first across all thresholds and influence metrics. Proximity Z-scores are unstable and reverse rankings between thresholds, failing to accurately reflect the physical distance advantage of Hyperforin.

Threshold	Compound	RWR Z	EWI Z	Proximity $d_c$	Proximity Z
$\geq 700$ (11,693 nodes)	Hyperforin	<b>+12.08</b>	+11.20	0.60	-6.04
	Quercetin	+5.53	+7.09	1.34	-5.46
$\geq 900$ (7,677 nodes)	Hyperforin	<b>+10.12</b>	+8.98	1.30	-3.86
	Quercetin	+4.55	+5.79	1.68	-5.44

Note: At  $\geq 900$ , Quercetin achieves a more "significant" proximity Z-score despite being physically more distant (1.68 vs 1.30) from DILI genes. RWR = random walk with restart; EWI = expression-weighted influence;  $d_c$  = mean minimum shortest-path distance; DILI = drug-induced liver injury.